

# Roles of Blackbody Friction Forces in the Rb and Cs Atom Interferometers

<sup>1</sup>Simranpreet Kaur, <sup>1</sup>Bindiya Arora,\* and <sup>2</sup>B. K. Sahoo

<sup>1</sup>*Department of Physics, Guru Nanak Dev University, Amritsar, Punjab 143005, India and*

<sup>2</sup>*Atomic, Molecular and Optical Physics Division,  
Physical Research Laboratory, Navrangpura, Ahmedabad 380009, India*

(Dated: December 15, 2020)

Atom interferometry is amongst the most advanced technologies that provides very high-precision measurements. There can exist a number of obscure forces that can interfere with the atoms used in this instrument. In the present work, we are probing possible roles of one such important forces, known as “blackbody friction force (BBFF)”, that may affect the precisions in the measurements made using atom interferometers based on the Rb and Cs atoms. The BBFF can be generated on atoms due to the black-body radiations emitted by the stray electromagnetic fields present in the experimental set-up and other metallic shielding. The strength of the BBFF can be calculated by integrating the complex parts of the dynamic polarizabilities of atoms, which show varying behaviour at the resonant and non-resonant transitions in the above atoms. Our analyses suggest that the off-resonant atomic transitions make significant contributions to the BBFF at low temperatures in the Rb and Cs atom interferometers. Present study also advocates that it is imperative to carry out the integration over a wide spectrum of frequencies for correct evaluation of the BBFF; specially at higher temperatures.

## I. INTRODUCTION

The non-contact friction forces have become a primary focus of research these days [1, 2]. Friction has been usually considered as a surface contact force. However, it has been revealed that friction can exist even between microscopic-bodies without making any physical contact at all. The thermal blackbody radiations contain a continuous spectrum of frequencies. When an atom encounters these radiations of disparate frequencies and wavelengths, it can experience a repulsive radiation pressure that will slow down the motion of the atom moving towards source and will bring it to the rest after a certain period of time; known as slowdown time. This repulsive force that acts in a direction opposite to the motion of an atom is usually called as blackbody friction force (BBFF). This is a special type of non-contact force, whose role in the high-precision measurements of atomic spectroscopies is not examined thoroughly but can be critical. Particularly, its effect may become prominent in the estimations of systematics in the ultra-high precision experiments like clock frequency measurements. Such interactions between the electromagnetic radiations and molecules are also expected to influence the behavior of molecules formed from the residue of novas and supernovas. As a result, the molecules in these astronomical objects can get subjected to a drag from numerous electromagnetic radiations that are present in the background and can act analogous to the blackbody radiations [3]. Therefore, it is important to fathom the effect due to BBFF on atoms and molecules in general.

It is determined that the aforementioned friction force on He atoms, in its  $^3S_1$  metastable state, can induce a slowdown time of 3016s ( $\approx 50$  minutes) at a temperature

corresponding to the melting point of tungsten (3695 K) [2]. It means that the presence of this force can affect the behaviour of clouds and interstellar dust in the space. Since the strength of BBFF on an atom depends directly on its dynamic electric dipole (E1) polarizabilities, the BBFF is also expected to influence strongly the polarizable atomic systems at some ambient temperature. This instigate to analyze the role of the BBFF in the high-precision measurements using instruments such as atom interferometers and quantum atom gravimeters [4], which are employed to carry out measurements of subtle effects like the detection of gravitational waves [5], testing general relativity [6], search for dark matter [7], Newtonian gravitational constant (G) [8], gravitational force [9, 10], etc. to name a few.

The basic working principle of any interferometer lies on the interference of two counter propagating waves. The optical interferometers combine two light waves to detect the tiny changes in the distance that they travel. Adhering to the same principle, the atom interferometers, in which a cloud of ultra-cold atoms is launched upwards with a quick pulse of laser light [11], probe the behaviors of de Broglie matter waves associated with the atoms [12]. The laser pulse in it is triggered in such a manner that it kicks off half of the atoms but without affecting the other half. When the two groups of these atoms meet again, their matter waves interfere. Their phase shift can be detected using the atom interferometers [13]. There could be a drift in the measurement of this tiny phase shift if the motion of the atoms in the interferometer is affected even slightly due to the friction forces exerted on them by the radiations emitted from the metallic shielding of the apparatus or other surroundings.

The most precise quantum gravimeters proposed till date perform atom interferometry with Rb atoms to measure the gravity gradients [14, 15]. In one such setup, tungsten cylinders are used as source masses, and their

---

\* bindiya.phy@gndu.ac.in

gravitational interactions with laser cooled Rb atoms are observed in order to determine the value of  $G$  [8]. It can be anticipated that there exists a change in speed of atoms caused by the BBFF exerted on them, originating from the radiations of tungsten cylinders and apparatus shielding. Therefore, it is necessary to investigate the role of BBFF on Rb atoms in order to reduce possible systematics in the measurement of  $G$  in this experiment. Furthermore future up-gradations of the Cs fountain atom interferometers are also being proposed to boost to the accuracy in the measurement of the fine structure constant [16], where BBFF may contribute to the systematics to a certain extent.

In this work, we intend to determine the effect of BBFF on the Rb and Cs atoms that are widely used in atom interferometers and quantum atom gravimeters these days. This may be useful when the precision of the measurements in the next-generation atom interferometers and other precision instruments reach to the higher levels. We would also like to demonstrate the temperature dependence of the characteristic slow down time associated with the BBFF for the above atoms.

The paper is organized as follows: In Sec. II, we present the theory used for calculation of the BBFF and the approach for evaluating the E1 polarizabilities that are required for accurate evaluation of these forces. In Sec. IV, we present the results related to the BBFF on the Rb and Cs atoms, and discuss their behaviors before concluding in the last section.

## II. EVALUATION APPROACH

Physically, the retardation of an atom due to the BBFF arising in an instrument can be understood by assuming that an atom moving towards the source of radiations absorb blue shifted photons from the direction of source, whereas the photons coming in from other direction are slightly red shifted and thus, less energetic. In contrast, the emission takes place symmetrically with respect to the forward and backward directions in the rest frame of the atom. So, the atom emits these photons in all possible directions, consequently suffering a net drain on its energy. Due to this, it loses its kinetic energy and as a consequence, it also experiences a drop in its momentum. This BBFF exerted on the atom closely resemble the thermal drag experienced by it while moving relative to a thermal photon bath [3].

Using correlation functions for the thermal electromagnetic fluctuations and employing the Green-Kubo formula [17, 18], an expression for BBFF acting on a single body (here it is an atom) moving relative to a thermal bath of the electromagnetic field excitations has been derived in literature [3] and is given by

$$F = -\frac{\beta \hbar^2 v}{3\pi c^5 (4\pi \epsilon_0)} \int_0^\infty \frac{\omega^5 \text{Im}[\alpha_0(\omega)]}{\sinh^2\left(\frac{\beta \hbar \omega}{2}\right)} d\omega, \quad (1)$$

where  $\beta = \frac{1}{k_B T}$  and  $\alpha_0(\omega)$  represents the dynamic E1

polarizability of the ground state of the atom (denoted by subscript 0). This expression corresponds to the thermal drag acting on the atom (generally moving with non-relativistic velocities) in a frame of reference where it is considered to be at rest and the photon gas is assumed to be moving with a velocity  $v$ . Clearly, Eq. (1) signifies that the BBFF has a strong dependence on the  $\alpha_0(\omega)$  values of the atom. Therefore, estimation of  $F$  demands for accurate evaluation of the  $\alpha_0(\omega)$  values for a sufficiently large range of frequencies  $\omega$ .

Determination of  $\alpha_0(\omega)$  values highly depend upon the off-resonant excitations with a broad non-negligible transition width  $\Gamma_n$  and also contain contributions from the near-resonance excitations involving very narrow  $\Gamma_n$  values. Since we are interested to evaluate these values from all ranges of spectra, we divide these values into two categories for the sake of convenience. In one part, these values involve contributions from the atomic transitions that are infinitely narrow and the value of  $\Gamma_n$  is small enough to be neglected. Then, these values are estimated by using the Dirac's prescription [2] as

$$\text{Im}[\alpha_0(\omega)] = \sum_n \frac{\pi f_{0n}}{2\omega_{0n}} \delta(\omega - \omega_{0n}), \quad (2)$$

where  $f_{0n}$  represents the oscillator strength of a transition associated with the ground state and another state with valence orbital denoted by  $n$ , which is a measure of probability of emission or absorption of the blackbody radiations,  $\omega_{0n}$  is the resonance frequency and  $\omega$  is the driving frequency. The  $\alpha_0(\omega)$  values at the non-resonant transitions can also be reasonably large and can contribute to some extent to the thermal friction on atoms. Evaluating  $\alpha_0(\omega)$  for the off-resonance transitions is relatively challenging compared to the values obtained at the near-resonant excitations as it requires to include the transition widths  $\Gamma_n$  in its formulation as [19]

$$\alpha_0(\omega) = \sum_n \sum_{\pm} \frac{f_{0n}}{2\omega_{0n}} \frac{1}{\omega_{0n} - \frac{i}{2} \frac{\omega^3 \Gamma_n(\omega)}{\omega_{0n}^3} \pm \omega}. \quad (3)$$

From the above expression, one can easily extract the imaginary part of polarizability by using the relation

$$\text{Im}[\alpha_0(\omega)] = \sum_n \frac{f_{0n} \Gamma_n(\omega) \omega_{0n}}{(\omega^2 - \omega_{0n}^2)^2 + \omega_{0n}^2 \Gamma_n^2(\omega)}. \quad (4)$$

Owing to finite transition width  $\Gamma_n(\omega)$  of the  $n^{\text{th}}$  energy level, the atomic transitions can be driven at a frequency far from resonance as well. Although the transition probabilities for such transitions are small yet not negligible [2]. The transition width in the above formula of dynamic polarizability is a function of driving frequency  $\omega$ . One can conveniently consider the approximation for the frequency dependent  $\Gamma_n(\omega)$  in terms of constant transition width  $\Gamma_n$  for a given  $n^{\text{th}}$  energy level as  $\Gamma_n(\omega) = \left(\frac{\omega}{\omega_{0n}}\right)^3 \Gamma_n$  in the length gauge. The transition width  $\Gamma_n$  for transition between the ground and  $n^{\text{th}}$

energy level is given as

$$\Gamma_n = \frac{2.02613 \times 10^{18} S_{n0}^{E1}}{\lambda^3 g_n}, \quad (5)$$

where  $\lambda$  is the transition wavelength,  $g_n = 2J_n + 1$  is the degeneracy factor with angular momentum  $J_n$  and  $S_{n0}^{E1}$  is the line strength due to the E1 matrix element given by  $S_{n0}^{E1} = |\langle J_n || \mathbf{D} || J_0 \rangle|^2$  for the E1 operator  $D$ . In the above expressions, the oscillator strength  $f_{0n}$  can be calculated as

$$f_{0n} = -\frac{303.757}{g_0 \lambda} S_{0n}^{E1}. \quad (6)$$

On filling Eqs. (4), (5) and (6) in Eq. (1), the expression for estimating strength of BBFF becomes quite intricate and is, thus, difficult to be worked out in its original form. Pondering over the complications involved in this expression, we follow the same approach used by the authors of Ref. [2], who have used a dimensionless model integral constructed by replacing the transition width  $\Gamma_n$ , driving frequency  $\omega$ , and  $\beta$  with their dimensionless equivalents as

$$\begin{aligned} \omega \rightarrow x &= \frac{\hbar\omega}{E_h}, & \beta \rightarrow \frac{\hbar\beta}{E_h} &= \frac{E_h}{K_B T}, \\ \Gamma_n \rightarrow \gamma_n &= \frac{\hbar\Gamma_n}{E_h}, & \text{and } \omega_{0n} \rightarrow x_{0n} &= \frac{\hbar\omega_{0n}}{E_h}. \end{aligned} \quad (7)$$

The entity  $E_h$  here represents the Hartree energy. By using the above assumptions, the expression for dynamic polarizability changes to

$$\alpha_0(x) = \frac{f_{0n}}{2x_{0n}} \frac{1}{x_{0n} \pm x - \frac{\gamma_n}{2} \left(\frac{x}{x_{0n}}\right)^3}. \quad (8)$$

Eventually, the imaginary component of the above formula reduces to

$$\text{Im}[\alpha_0(x)] = \sum_{\pm} \frac{f_{0n}}{2x_{0n}} \frac{\gamma_n}{2} \frac{x^3}{x_{0n}^3} \frac{1}{(x_{0n} \pm x)^2 + \frac{\gamma_n^2}{4} \left(\frac{x}{x_{0n}}\right)^6}. \quad (9)$$

Interestingly, on employing the dimensionless counterparts and using a function  $e^{-bx}$  to model the hyperbolic sine in denominator of the integrand of Eq. (1), the final form of integral reduces to

$$J = \int_0^{\infty} x^5 e^{-bx} \text{Im}[\alpha_0(x)] dx. \quad (10)$$

The value of  $J$  in the above expression for BBFF further depends upon the form of imaginary polarizability under consideration. If we consider the one representing the near resonant contribution as shown in Eq. (2), after applying properties of a Dirac-delta function,  $J$  simply changes to

$$J = \frac{\pi f_{0n}}{2x_{0n}} x_{0n}^5 e^{-bx_{0n}}. \quad (11)$$

However, if we choose the  $\gamma_n$  dependent imaginary component of dynamic polarizability as given in Eq. (9), then  $J$  comes out to be

$$J = \int_0^{\infty} \sum_{\pm} \frac{f_{0n}}{2x_{0n}} \frac{\gamma_n}{2} \frac{x^3}{x_{0n}^3} \frac{x^5 e^{-bx}}{(x_{0n} \pm x)^2 + \frac{\gamma_n^2}{4} \left(\frac{x}{x_{0n}}\right)^6} dx. \quad (12)$$

Finally, on substituting all these newly deduced formulations, the expression for BBFF simplifies to

$$F = -\frac{\beta \hbar^2 v}{3\pi c^5 (4\pi \epsilon_0)} J. \quad (13)$$

In order to have a better understanding of the behaviour of BBFF, we are going to consider two different choices of integration limits in Eq. 12. In one case, we will take the integration limits of  $\omega$ , i.e.  $x$  from 0 to  $x_{0n} - \frac{\gamma_n}{2}$ , where  $\gamma_n$  represents the decay width of the  $n^{\text{th}}$  energy level corresponding to energy  $x_{0n}$  as done by the authors of Ref. [2]. In the second case, we take the integration limits over a wide spectrum of frequencies, ranging from 0 to a very large value. The results for both the cases have been discussed latter.

### III. METHOD OF CALCULATIONS

We evaluate the E1 polarizabilities by dividing total contributions from different intermediate states as

$$\alpha_0 = \alpha_0^c + \alpha_0^{vc} + \alpha_0^v, \quad (14)$$

where the superscripts  $c$ ,  $vc$  and  $v$  correspond to core contributions due to the inner intermediate states without interacting with valence orbital, core-valence contribution due to the inner core states interacting with valence orbital and valence contributions due to upper intermediate states, respectively. The valence contribution is further divided into two parts: contributions arising from the low-lying intermediate bound states (referred to as ‘‘Main’’ contribution) and from the remaining states including continuum (denoted as ‘‘Tail’’ contribution). This helps us to evaluate the ‘‘Main’’ contribution more precisely by using the experimental energies and calculating the E1 matrix elements accurately by employing a relativistic all-order many-body method in the sum-over-states approach using the formula [20]

$$\alpha_0^{v,\text{Main}}(\omega) = \sum_{n \neq 0}^K \frac{f_{0n}}{2\omega_{0n}} \left[ \frac{1}{\omega_{0n} - \mathcal{L} + \omega} + \frac{1}{\omega_{0n} - \mathcal{L} - \omega} \right] \quad (15)$$

where  $\mathcal{L} = \frac{v}{2} \frac{\omega^3 \Gamma_n}{\omega_{0n}^3}$ ,  $f_{0n} = -\frac{303.757}{g_0 \lambda} |\langle J_0 || \mathbf{D} || J_n \rangle|^2$  and  $K$  represents number of intermediate bound states included. In our work, we have included the contributions from  $K = 8$  and  $K = 9$  excited states for the evaluation of E1 polarizabilities of the Rb and Cs atoms, respectively, to estimate the BBFF precisely. The all-order relativistic method employed here to determine the atomic states

and their matrix elements is discussed in Refs. [21–24] and is described briefly below.

In our method, the wave function for any state with a valence orbital  $v$  is expressed as

$$|\Psi_v\rangle_{\text{SD}} = \left[ 1 + \sum_{ma} \rho_{ma} a_m^\dagger a_a + \frac{1}{2} \sum_{mpab} \rho_{mpab} a_m^\dagger a_p^\dagger a_b a_a + \sum_{m \neq v} \rho_{mv} a_m^\dagger a_v + \sum_{mpa} \rho_{mpva} a_m^\dagger a_p^\dagger a_a a_v \right] |\Phi_v\rangle, \quad (16)$$

where  $|\Phi_v\rangle$  is the mean-field wave function defined as  $|\Phi_v\rangle = a_v^\dagger |0_c\rangle$  with  $|0_c\rangle$  as the Dirac-Hartree-Fock (DHF) wave function of the closed core of the respective atom,  $a^\dagger$  and  $a$  are the second quantization operators with subscripts  $a, b$  and  $p, m$  denoting occupied and virtual orbitals respectively. In the above expression, the subscript SD denotes only the singly and doubly excited configurations are considered in which the quantities  $\rho_{ma}$  and  $\rho_{mv}$  are the one-hole–one-particle excitation amplitudes without involving valence orbital and involving valence orbital respectively, and the quantities  $\rho_{mpab}$  and  $\rho_{mpva}$  are the two-hole–two-particle excitation amplitudes without involving valence orbital and involving valence orbital respectively. These amplitudes are obtained by solving the many-body Schrödinger equation through iterative procedure till self-consistent solutions are attained. The single particle wave functions in the DHF method are constructed by a finite basis set using the B-splines [25]. In this work, we have used 70 splines of order  $k = 11$  for each angular momentum and the radial functions are defined on a non-linear grid by constraining to a large spherical cavity of a radius  $R = 220$  in atomic units (a.u.).

After determining the atomic wave functions, the reduced E1 matrix element between the states  $|\Psi_n\rangle$  and  $|\Psi_m\rangle$  is calculated by

$$M_{nm} = \frac{\langle J_n || \mathbf{D} || J_m \rangle}{\sqrt{\langle \Psi_n | \Psi_n \rangle \langle \Psi_m | \Psi_m \rangle}}. \quad (17)$$

The calculated E1 matrix elements using this expression combining with the experimental energies give rise to “Main” contributions to the E1 polarizabilities. Since “Tail” contributions to  $\alpha_0^v$  are much smaller than the “Main” contribution, we have estimated them by using the matrix elements from the DHF method in the sum-over-states approach. The core and core-valence contributions are also relatively smaller, so they have been estimated using the DHF method.

#### IV. RESULTS AND DISCUSSION

In order to probe the effect of the BBFF on the Rb and Cs atoms that conventionally serve in atom interferometers, we first discuss the results of our oscillator strengths,

TABLE I. Comparison of our calculated values of the absorption oscillator strengths ( $f_{0n}$ ) for the first four  $5S_{1/2} \rightarrow nP_{1/2,3/2}$  and  $6S_{1/2} \rightarrow nP_{1/2,3/2}$  transitions of the Rb and Cs atoms, respectively, with the NIST data [26]. The transition frequencies ( $\omega_{0n}$ ) and linewidths ( $\Gamma_n$ ) for transitions from upper to lower state are also given. The integers (e.g.  $[k]$ ) shown in the square brackets in the last two columns represent exponent of 10 (e.g.  $\times 10^k$ ).

Transition		$\omega_{0n}$ (in a.u.)	$f_{0n}$	$f_{0n}$ [26]	$\Gamma_n$ (in $s^{-1}$ )
lower(0)	upper (n)				
Rb atom					
$5S_{1/2}$	$5P_{1/2}$	0.057	3.402[-1]	3.420[-1]	3.591[7]
$5S_{1/2}$	$5P_{3/2}$	0.058	6.902[-1]	6.950[-1]	3.781[7]
$5S_{1/2}$	$6P_{1/2}$	0.108	4.006[-3]	4.000[-3]	1.503[6]
$5S_{1/2}$	$6P_{3/2}$	0.108	1.056[-2]	0.938[-2]	1.995[6]
$5S_{1/2}$	$7P_{1/2}$	0.127	5.581[-4]	0.559[-3]	2.884[5]
$5S_{1/2}$	$7P_{3/2}$	0.127	1.732[-3]	1.530[-3]	4.487[5]
$5S_{1/2}$	$8P_{1/2}$	0.136	1.600[-4]	1.500[-4]	9.525[4]
$5S_{1/2}$	$8P_{3/2}$	0.136	5.586[-4]	4.610[-4]	1.661[5]
Cs atom					
$6S_{1/2}$	$6P_{1/2}$	0.051	3.409[-1]	3.435[-1]	2.842[7]
$6S_{1/2}$	$6P_{3/2}$	0.053	7.081[-1]	7.142[-1]	3.251[7]
$6S_{1/2}$	$7P_{1/2}$	0.099	2.908[-3]	2.510[-3]	9.189[5]
$6S_{1/2}$	$7P_{3/2}$	0.099	1.203[-2]	1.143[-2]	1.933[6]
$6S_{1/2}$	$8P_{1/2}$	0.117	3.205[-4]	2.040[-4]	1.413[5]
$6S_{1/2}$	$8P_{3/2}$	0.118	2.102[-3]	1.740[-3]	4.665[5]
$6S_{1/2}$	$9P_{1/2}$	0.126	8.052[-5]	4.400[-5]	4.103[4]
$6S_{1/2}$	$9P_{3/2}$	0.126	7.594[-4]	5.600[-4]	1.941[5]

transition widths and polarizability calculations for the Rb and Cs atoms below. Then, we discuss about the roles of the high-lying states, off-resonant and resonant transitions and integration limits on the determination of the BBFFs in both the considered atoms.

Table I summarizes the transition frequencies and oscillator strength data for the first eight atomic transitions of Rb and Cs atoms. Transition widths for these first eight excited states have also been presented in the same table. Experimental values of the transition frequencies from the National Institute of Science and Technology (NIST) database [26] have been taken in our calculations. The matrix elements required to determine the oscillator strengths and transition widths given in the table were calculated using the relativistic all-order method described in the previous section. We compare oscillator strengths calculated using our method with the data available on the NIST database [26]. We find that our calculated values of transition probabilities for the primary transitions are in good agreement with the values quoted on the NIST database. Although, there are some subtle discrepancies in the values for higher transitions, but they do not contribute much to our overall results.

In the foregoing, we present results for the static dipole polarizabilities of the ground state  $5S_{1/2}$  for Rb and  $6S_{1/2}$



TABLE II. Static dipole polarizabilities ( $\alpha_0$ ) of the ground states of Rb ( $5S_{1/2}$ ) and Cs ( $6S_{1/2}$ ) atoms (in a.u.). We have shown the contributions from individual transitions and have also compared our values with available experimental data. Uncertainties are given in the parentheses. To reduce the uncertainties in the evaluation of  $\alpha_0$ , we have used precise values of E1 matrix elements of the principal transitions by inferring from the experiments [27–29].

Rb			Cs		
Transition	E1 Matrix Elements	Contribution to $\alpha_{0,v}$	Transition	E1 Matrix Elements	Contribution to $\alpha_{0,v}$
$5S_{1/2} \rightarrow 5P_{1/2}$	4.231(3) [27]	104.1(2)	$6S_{1/2} \rightarrow 6P_{1/2}$	4.498(6) [28]	132.4(4)
$5S_{1/2} \rightarrow 6P_{1/2}$	0.334	0.343	$6S_{1/2} \rightarrow 7P_{1/2}$	0.297	0.296
$5S_{1/2} \rightarrow 7P_{1/2}$	0.115	0.035	$6S_{1/2} \rightarrow 8P_{1/2}$	0.091	0.023
$5S_{1/2} \rightarrow 8P_{1/2}$	0.059	0.009	$6S_{1/2} \rightarrow 9P_{1/2}$	0.044	0.005
$5S_{1/2} \rightarrow 5P_{3/2}$	5.978(5) [27]	204.0(3)	$6S_{1/2} \rightarrow 6P_{3/2}$	6.335(5) [29]	250.2(4)
$5S_{1/2} \rightarrow 6P_{3/2}$	0.541	0.899	$6S_{1/2} \rightarrow 7P_{3/2}$	0.601	1.204
$5S_{1/2} \rightarrow 7P_{3/2}$	0.202	0.107	$6S_{1/2} \rightarrow 8P_{3/2}$	0.232	0.152
$5S_{1/2} \rightarrow 8P_{3/2}$	0.111	0.030	$6S_{1/2} \rightarrow 9P_{3/2}$	0.134	0.048
$\alpha_{0,v}$ (Main)		309.5(4)	$\alpha_{0,v}$ (Main)		384.3(5)
$\alpha_{0,v}$ (Tail)		0.14(1)	$\alpha_{0,v}$ (Tail)		0.22(2)
$\alpha_{0,vc}$		-0.26( $\sim$ 0)	$\alpha_{0,vc}$		-0.47( $\sim$ 0)
$\alpha_{0,c}$		9.1(5)	$\alpha_{0,c}$		15.8(3)
Total ( $\alpha_0$ )		318.5(6)	Total ( $\alpha_0$ )		399.9(6)
Experiment		319.8(3) [30]	Experiment		400.8(4) [30]

for Cs and compare them further with the previously available experimental and theoretical results in Table II. Since valence correlation contributions  $\alpha_{0,v}$  are vital for accurate estimate of polarizabilities, we include the E1 matrix elements among the low-lying states up to the  $5S_{1/2} - 8P_{1/2,3/2}$  and the  $6S_{1/2} - 9P_{1/2,3/2}$  transitions in Rb and Cs respectively and refer them as the “Main” part of  $\alpha_{0,v}$ . We replaced some of the matrix elements with the more accurate experimental values wherever available to improve the accuracies of the results. To be precise, we have replaced the matrix elements corresponding to  $5S_{1/2} \rightarrow 5P_{1/2,3/2}$  transitions in Rb [27] and those of  $6S_{1/2} \rightarrow 6P_{1/2,3/2}$  transitions in Cs [28, 29] with their experimentally calculated values. We also give contributions from the core-valence  $\alpha_{0,vc}$  and core  $\alpha_{0,c}$  contributions to our calculations in this table. Our calculated values of E1 polarizabilities for the ground state of Cs is 399.5 in atomic units (a.u.) and it is 318.3 a.u for Rb. This matches very well with the experimentally measured value of 400.8 a.u and 319.3 a.u for Cs and Rb. [30]. The measurement of the ground state dipole polarizability of Rb using a Mach-Zehnder atom interferometer with an electric-field gradient was conducted by the authors of Ref. [31]. Our estimated value agrees quite well with this value also. Similarly, results for both the atoms are in good agreement with the values reported in Ref. [32].

Following the techniques mentioned in the previous section of this paper, the values of the slowdown time for both the considered atoms have been calculated over a wide range of temperatures and presented in graphical form. As BBFF has a major dependence on the value of dynamic polarizability, so the BBFF and correspondingly the slowdown time also enjoy major contributions from

the primary transitions only. Abiding by this prevalent trend of reducing contributions with increasing values of intermediate state, the BBFF due to the transitions from the  $5S_{1/2}$  state to the  $6P_{1/2}$  and  $6P_{3/2}$  states have been found to be dominating in case of Rb atoms. Similarly, contributions from the transitions involving the  $6S_{1/2}$  and  $7P_{1/2,3/2}$  states show major influence in case of Cs atoms. For example, at a driving frequency of 0.025 a.u. for Rb atoms,  $Im[\alpha(\omega)]$  for the  $5S_{1/2} \rightarrow 5P_{1/2}$  transition comes out to be of the order of  $10^{-7}$  a.u., while this value reduces to  $10^{-15}$  a.u. for the  $5S_{1/2} \rightarrow 8P_{3/2}$  transition.

Figs. 1 and 2, on the whole depict the variation of slowdown time  $\tau$  arising due to the BBFF acting on the Rb and Cs atoms with respect to the temperature T of the source emitting the radiations. The slowdown time plotted here is in years while the temperature of the source is in Kelvins. As a moving atom comes in the vicinity of these friction forces acting on it, it slows down which subsequently gives rise to a characteristic slowdown time,  $\tau$ . This characteristic slowdown time is inversely related to the magnitude of the BBFF experienced by the atoms as  $\tau = \frac{mv}{F}$ .

We found that the choice of integration limits can also induce significant changes in our results at higher temperature. Thus, we make case-wise analysis depending upon the findings with the the limits of the integration to explain the underlying behaviors. The dashed lines represent as “Case I” study, which highlight the behaviour of slowdown time  $\tau$  with temperature T when linewidth  $\Gamma_n$  is not included in the calculation of polarizability. To plot this behaviour without taking into account the influence of linewidth of atomic levels, the Dirac-delta formulation of imaginary part of polarizability, given by

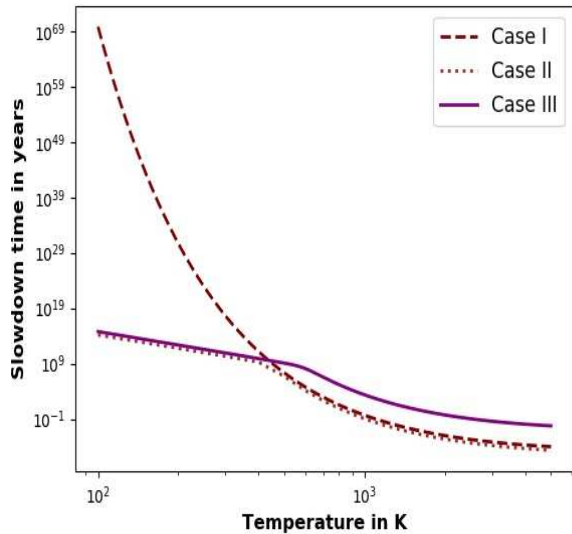


FIG. 1. The variation of slowdown time  $\tau$  with temperature  $T$  for different conditions of driving frequency  $\omega$  and integration limits for Rb atoms. Here, the curve titled “Case I” represents the results for near resonance transitions, plotted using Eq. 11. The variations shown corresponding to “Case II and Case III” convey the behaviour shown at the off-resonance frequencies. In Case II, the graph has been plotted by taking the integration limits as  $0 < \omega < \omega_{0n} - \frac{\Gamma_n}{2}$  in Eq. (10), whereas Case III involves a wider set of integration limits as  $0 < \omega < 3000$  a.u..

Eq. (9), was employed. In this case, the slowdown time has been observed to follow a continuous exponential decay in its value with the increasing values of temperature for both the atoms. The plots named as Case II and Case III show contributions from the non-resonant transitions by considering different choices of integration limits. The dotted curve associated with Case II represents the variation when the driving frequency ranges from 0 to slightly less than the resonance frequency. Precisely,  $\omega$  in this case lies between 0 to  $\omega_{0n} - \frac{\Gamma_n}{2}$ . However, in Case III, we have tried to accommodate a wider set of integration limits. Here, the driving frequency ranges from 0 to a very high value, and the slowdown time varies as indicated by the solid lines. With a set of narrower integration limits in Case II, the graph exits the linear behaviour and makes a transition to exponential decay at a lower temperature and almost coincides with the graph plotted for near-resonance transitions. However, in the latter case, this shift occurs at a slightly higher temperature, without completely coinciding with the graph plotted using the Dirac-delta function. For Rb atoms, the shift from linear to exponential behaviour for  $0 < \omega < \omega_{0n}$  occurs near 410 K. However, the graph exhibits the linearly decreasing behaviour near 545 K for very large limits of  $\omega$ . In the case of Cs atoms, these transitions occur near 395 K and 620 K. It is worth noting that at lower temperatures, the

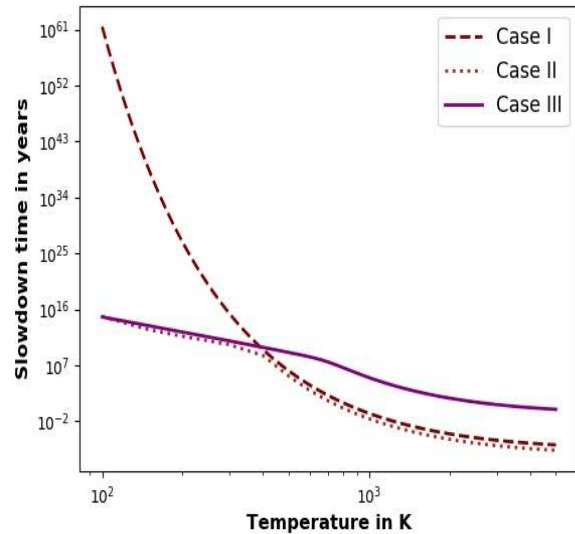


FIG. 2. The variation of slowdown time  $\tau$  with temperature  $T$  for different conditions of driving frequency  $\omega$  and integration limits for Cs atoms. Case I, Case II and Case III hold the same significance as in Fig. 1 shown for the Rb atom.

choice of integration limits does not affect significantly. Due to this the dotted and solid curves coincide at lower temperatures for both the atoms.

The graphs depicted in Figs. 1 and 2 also reveal that at lower temperatures, there exists a visible difference in the amount of friction force resulting separately from both the approaches. When we only consider the resonant frequencies, the value of slowdown time is quite large, approximately  $10^{69}$  years for Rb and  $10^{61}$  years for Cs at around 100K. This makes the BBFF quite negligible to be felt. However, if we involve the contribution of  $\Gamma_n$  by considering the off-resonant contributions, the values of slowdown show a significant decrease by orders of more than 45, which makes the BBFF quite noticeable to be taken into account. Furthermore, the difference between  $\tau$  calculated after including the near-resonant and off-resonant contributions reduces significantly and it becomes almost zero as the temperature increases implying that both the values come closer. At higher temperatures, the values of slowdown time almost stabilize and do not vary much with  $T$ .

We support the aforementioned observation by analyzing the variation of the integrand, given in Eq. (10), with the driving frequency  $\omega$  or  $x$  at two notably different temperatures. In Fig. 3, it is clear that the integrand is having a peak value, almost equal to  $10^{-21}$  at the off-resonance frequencies. Thereafter, it decreases but again shows a sharp increase to  $10^{-27}$  at 0.050931 a.u. and 0.05731 a.u., which basically correspond to the resonance frequencies of the first low-lying transitions in the Cs and Rb atoms respectively. It is evident from this that at low temperatures near 300K, the contribution to the

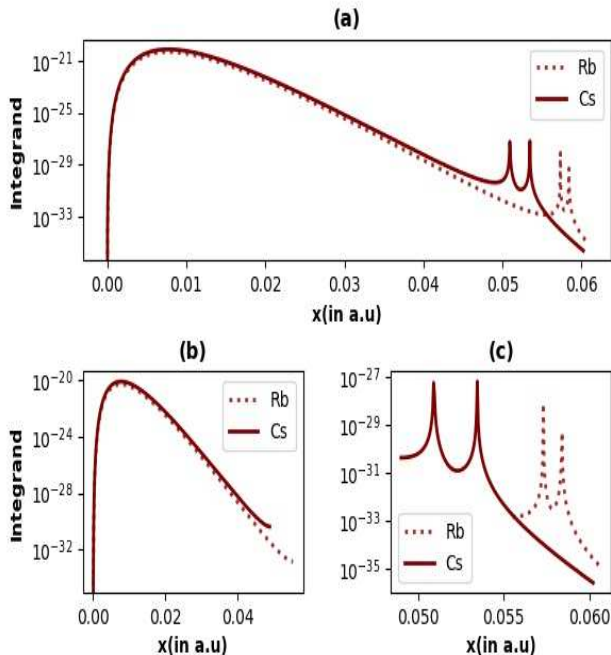


FIG. 3. Variation of the integrand ( $x^5 e^{-bx} \text{Im}[\alpha_0 x]$ ) with driving frequency  $x$  at low temperature (300K) for both the Rb (dotted line) and Cs (solid line) atoms. We have provided an overall picture of variation in values of the integrand (a) over an entire spectrum of driving frequencies, along with a zoomed out view of variation at the (b) off-resonance and (c) near resonance frequencies.

integrand made by the near-resonance and off-resonance transitions differ by a factor of 6, and the off-resonance transitions are the ones that dominate the overall calculations of the BBFF. These values of integrand correspond to a slowdown time of  $10^{15}$  and  $10^{17}$  years for both the Rb and Cs atoms coming from the resonant transitions and a slowdown time  $10^{10}$  years for both the atoms coming from the off-resonant transitions. However, this trend is quite opposite at the higher temperatures, as seen in Fig. 4. At the higher temperatures, say 5000K, the peak seems to occur at the resonant frequencies only and there are no major contributions to the values of the integrand at the off-resonance frequencies. This makes the inclusion of transition width  $\Gamma_n$  insignificant to the calculation of the BBFF at the higher temperatures.

From the calculated values of slowdown time, one can further estimate the deceleration experienced by the atoms by simply employing the relation  $a = \frac{v}{\tau}$ , where,  $v$  is the velocity with which the atoms are moving and  $\tau$  is the slowdown time as calculated earlier. Typically, the experiments aiming to conduct high-precision measurements, like that of equivalence principle, have atoms traveling at an average speed of  $10 \text{ ms}^{-1}$ . So, when the source of blackbody radiations is at room temperature, say 300K, the BBFF appears to decelerate both the Rb

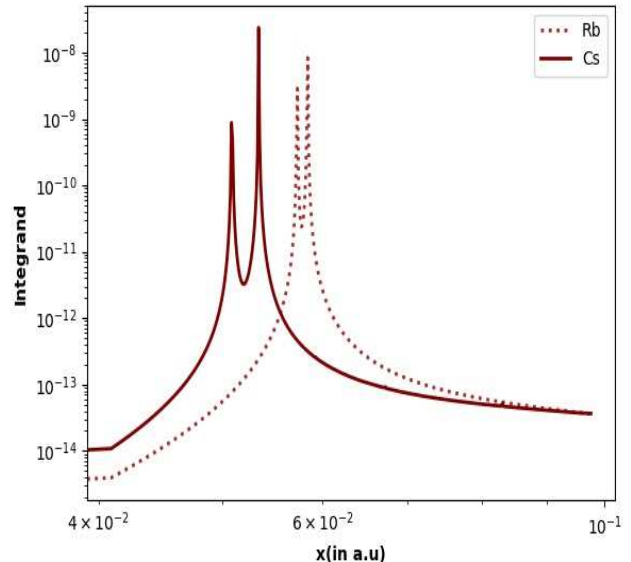


FIG. 4. Variation of the integrand ( $x^5 e^{-bx} \text{Im}[\alpha_0 x]$ ) with driving frequency  $x$  at high temperature (5000K) for both the Rb (dotted line) and Cs (solid line) atoms. Here, the peaks appear to occur only at near-transition frequencies and there is almost no contribution to the value of integrand from off-resonance transitions, contrary to the behaviour seen at low temperatures.

and Cs atoms by an order of  $10^{-17} \text{ms}^{-2}$ , corresponding to a slowdown time of  $10^{10}$  years.

## V. CONCLUSION

We have investigated the characteristics of the blackbody friction force which can play an important role in high-precision measurements using the atomic interferometers; especially considering the Rb and Cs atoms. Our analysis demonstrates that the dominant contribution to this force comes from the primary atomic transitions only. We also find that the inclusion of transition width  $\Gamma_n$  in the calculations shows notable contributions at low temperatures, which makes the transition width even more important to be taken into consideration while calculating the blackbody radiation force for those arrangements that operate at low temperatures. Moreover, we realized that these forces can decelerate the Rb and Cs atoms by  $10^{-17} \text{ms}^{-2}$ . Although this number appears quite negligible to be taken into account, still, a deceleration of this order can turn out to be a cause of concern for estimating possible systematic errors in future high-precision instruments aimed at measuring the values of fundamental constants and in the detection of gravitational waves. Such analyses can also be made in other atomic systems that are under consideration for precision experiments to estimate possible systematics due to the

blackbody friction force.

many important issues related to measurements in atom interferometry.

### ACKNOWLEDGEMENT

The authors are grateful to Dr. Holger Müller and Dr. Amar Vutha for useful discussions and clarifying

- 
- [1] A. I. Volokitin, *Jetp Lett.* **101**, 427 (2015).
- [2] G. Lach, M. DeKieviet, and U. D. Jentschura, *Phys. Rev. Lett.* **108**, 043005 (2012).
- [3] V. Mkrtchian, V. A. Parsegian, R. Podgornik, and W. M. Saslow, *Phys. Rev. Lett.* **91**, 220801 (2003).
- [4] V. Ménoret et al., *Sci Rep.* **8**, 12300 (2018).
- [5] P. W. Graham, J. M. Hogan, M. A. Kasevich, and S. Rajendran, *Phys. Rev. Lett.* **110**, 171102 (2013).
- [6] S. Dimopoulos, P. W. Graham, J. M. Hogan, and M. A. Kasevich, *Phys. Rev. Lett.* **98**, 111102 (2007).
- [7] P. Hamilton, M. Jaffe, P. Haslinger, Q. Simmons, H. Müller, and J. Khoury, *Science* **349**, 849 (2015), <https://science.sciencemag.org/content/349/6250/849.full.pdf>
- [8] G. Lamporesi, A. Bertoldi, L. Cacciapuoti, M. Prevedelli, and G. M. Tino, *Phys. Rev. Lett.* **100**, 050801 (2008).
- [9] G. Tino, F. Sorrentino, D. Aguilera, B. Battelier, A. Bertoldi, Q. Bodart, K. Bongs, P. Bouyer, C. Braxmaier, L. Cacciapuoti, N. Gaaloul, N. Gürlebeck, M. Hauth, S. Herrmann, M. Krutzik, A. Kubelka, A. Landragin, A. Milke, A. Peters, E. Rasel, E. Rocco, C. Schubert, T. Schuldt, K. Sengstock, and A. Wicht, *Nuclear Physics B - Proceedings Supplements* **243-244**, 203 (2012), proceedings of the IV International Conference on Particle and Fundamental Physics in Space.
- [10] J. M. McGuirk, G. T. Foster, J. B. Fixler, M. J. Snadden, and M. A. Kasevich, *Phys. Rev. A* **65**, 033608 (2002).
- [11] M. Zhan, K. Li, P. Wang, L. Kong, X. Wang, R. Li, X. Tu, L. He, J. Wang, and B. Lu, *Journal of Physics: Conference Series* **80**, 012047 (2007).
- [12] A. B. Barrett and P. Bouyer, *Phys. Scr.* **91**, 012047 (2016), [10.1088/0031-8949/91/5/053006](https://doi.org/10.1088/0031-8949/91/5/053006).
- [13] P. Hannaford, *Current Science* **67**, 276 (1994).
- [14] I. Perrin, Y. Bidel, N. Zahzam, C. Blanchard, A. Bresson, and M. Cadoret, *Phys. Rev. A* **99**, 013601 (2019).
- [15] B. Barrett, I. Chan, and A. Kumarakrishnan, *Phys. Rev. A* **84**, 063623 (2011).
- [16] R. Bouchendiria, P. Cladé, S. Guellati-Khélifa, F. Nez, and F. Biraben, *Phys. Rev. Lett.* **106**, 080801 (2011).
- [17] S. M. Rytov, Y. A. Kravtsov, and V. I. Tatarskii, *Principles of Statistical Radiophysics 3* (Springer-Verlag Berlin Heidelberg, 1989).
- [18] E. M. Lifshitz, L. P. Pitaevskii, and B. R. A. Nyboer, *Book-Review - Statistical Physics - Part Two* (Pergamon Press, Oxford, UK, 1958).
- [19] R. Loudon, *The Quantum Theory of Light* (Clarendon Press, Oxford, 1993).
- [20] M. S. Safronova and C. W. Clark, *Phys. Rev. A* **69**, 040501(R) (2004).
- [21] S. A. Blundell, W. R. Johnson, and J. Sapirstein, *Phys. Rev. A* **43**, 3407 (1991).
- [22] M. S. Safronova and W. R. Johnson, *Advances in Atomic Molecular and Optical Physics* **55**, 191 (2008).
- [23] B. K. Sahoo, D. K. Nandy, B. P. Das, and Y. Sakemi, *Phys. Rev. A* **91**, 042507 (2015).
- [24] B. K. Sahoo and B. P. Das, *Phys. Rev. A* **92**, 052511 (2015).
- [25] W. R. Johnson, S. A. Blundell, and J. Sapirstein, *Phys. Rev. A* **37**, 307 (1988).
- [26] A. Kramida, Y. Ralchenko, J. Reader, and N. A. T. (2012), “Nist atomic spectra database,” (version 5). [Online]. Available: <http://physics.nist.gov/asd> [2012, December 12]. National Institute of Standards and Technology, Gaithersburg, MD.
- [27] U. Volz and H. Schmoranzler, *Physica Scripta* **T65**, 48 (1996).
- [28] R. J. Rafac, C. E. Tanner, A. E. Livingston, K. W. Kukla, H. G. Berry, and C. A. Kurtz, *Phys. Rev. A* **50**, R1976 (1994).
- [29] B. M. Patterson, J. F. Sell, T. Ehrenreich, M. A. Gearba, G. M. Brooke, J. Scoville, and R. J. Knize, *Phys. Rev. A* **91**, 012506 (2015).
- [30] M. Gregoire, N. Brooks, R. Trubko, and A. Cronin, *Atoms* **4**, 21 (2016).
- [31] W. F. Holmgren, M. C. Revelle, V. P. A. Lonij, and A. D. Cronin, *Phys. Rev. A* **81**, 053607 (2010).
- [32] P. Schwerdtfeger and J. K. Nagle, *Molecular Physics* **117**, 1200 (2019).